Calculation of Circulating Bearing Currents in Machines of Inverter-Based Drive Systems

Annette Muetze, *Member, IEEE*, and Andreas Binder, *Senior Member, IEEE*

Abstract—The high-frequency circulating bearing current that may occur in machines of inverter-based drive systems can be described by an eddy-current model. The parameters of an equivalent circuit are derived from the model. The ratio between bearing current and common-mode current amplitudes for different machines is calculated. The theoretical maximum ratio is about 0.35. Copper loops applied for bearing current measurement may decrease the circulating bearing currents up to almost 40%.

Index Terms—Common-mode voltage, inverter-induced circulating bearing currents, variable-speed drives.

I. INTRODUCTION

FAST-SWITCHING insulated gate bipolar transistor inverters may cause additional bearing currents in inverter-based drive systems. The high-frequency circulating bearing current is one of the different principal contributing phenomena. It occurs in addition to the "classical" bearing current due to magnetic asymmetries of large line-fed motors. The inverter-induced circulating bearing currents follow the same path as the "classical" ones; yet, their origin is very different [1]–[8].

If no additional measures such as the use of filters or chokes that are designed for use in the inverter output are taken, the inverter is a common-mode voltage source that exposes the motor terminals to high dv/dt. This causes an additional high-frequency common-mode current $I_{\rm com}$, mainly because of the interaction of the high dv/dt at the motor terminals and the capacitance between motor winding and frame $C_{\rm wf}$. The frequencies of these high-frequency common-mode currents range from 100 kHz up to several megahertz [9].

In conventional machines, if no mitigation methods such as additional conductive shielding in the stator slots [10] are applied, the common-mode current excites a circumferential magnetic flux ("ring flux" or "common-mode flux") around the motor shaft. This flux induces a shaft voltage $v_{\rm sh}$ along the shaft of the motor. If $v_{\rm sh}$ is large enough to puncture

A. Muetze was with the Department of Electrical and Computer Engineering, University of Wisconsin, Madison, WI 53706-1691 USA. She is now with the School of Engineering, University of Warwick, Coventry CV4 7AL, U.K. (e-mail: a.muetze@warwick.ac.uk).

A. Binder is with the Institute of Electrical Energy Conversion, Darmstadt University of Technology, 64283 Darmstadt, Germany (e-mail: abinder@ew.tu-darmstadt.de).

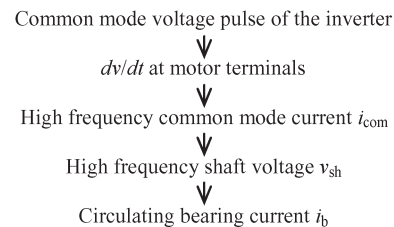**Inverter-induced circulating bearing currents**

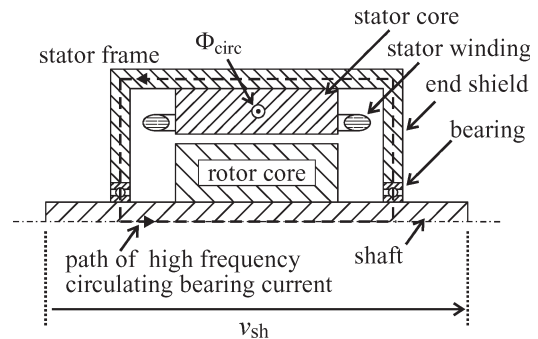Fig. 1. Mechanism of inverter-induced circulating bearing currents.

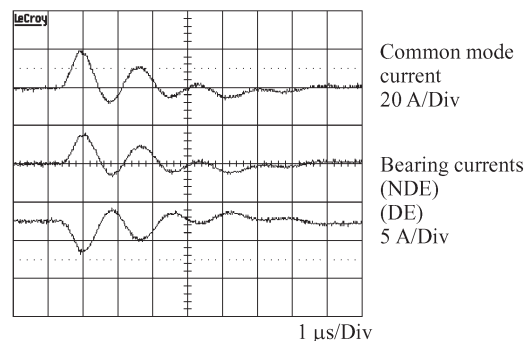Fig. 2. Path of high-frequency circulating bearing current.

Fig. 3. Circulating bearing currents, induction motor, 400-mm frame size, 500-kW rated power, motor speed $n = 3000$ r/min, and bearing temperature $\vartheta_{\rm b} \approx 70\,^{\circ}{\rm C}$.

the lubricating film of the bearing and destroy its insulating properties, it causes a circulating bearing current $i_{\rm b}$ along the loop "stator frame–nondrive end–shaft–drive end." Because this type of bearing current is due to inductive coupling, it mirrors the common-mode current. It is of opposite direction in both bearings (Figs. 1–3). Peak bearing current amplitudes $\hat{\imath}_{\rm b}$ vary—depending on the motor size—i.e., $\hat{\imath}_{\rm b} \approx 0.5-20$ A (power rating up to $P_{\rm r} = 500$ kW).
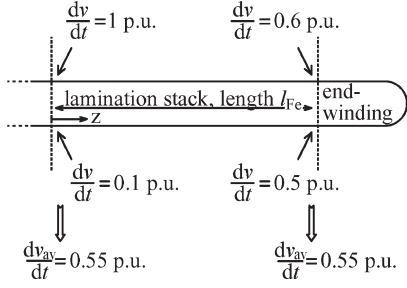
Fig. 4. Sketch of one turn of stator winding and distribution of dv/dt along the stack length.

II. CALCULATION OF COMMON-MODE RING FLUX

If no mitigation methods such as additional conductive shielding in the stator slots [10] are applied, the common-mode current i_{com} excites the high-frequency common-mode flux Φ_0, which can induce high-frequency circulating bearing currents. Without the use of additional special measures, the current enters the machine via the stator windings and leaves through the grounding connection(s) of the motor, thereby passing the stator stack lamination. Understanding of the resultant generation of the common-mode flux is essential for the comprehension of the circulating bearing current phenomenon. Important work in this field is reported in [11] and [12], which is used here as a starting point.

The current distribution in the stator lamination can be described by an eddy-current model with sinusoidal variation of the parameters with respect to the time. The stator lamination stack is represented by a 2-D model with cylindrical symmetry, using the cylindrical coordinate system (r, φ, z). The common-mode flux is supposed to flow in the azimuthal direction, i.e., $\vec{\underline{H}} = (0, \underline{H}_\varphi(r,z), 0)$. The current density has only an r-component and a z-component, i.e., $\vec{\underline{J}} = (\underline{J}_r(r,z), 0, \underline{J}_z(r,z))$. The laminations of the stator stack are insulated from each other by a coating. It is assumed that the contact impedance between the laminations and the stator frame is very small and that the conductivity of the lamination sheets is significantly larger than the conductivity of the frame. Furthermore, it is supposed that the circumferential flux flows mainly in the cylindrical part of the stator lamination stack, which is the so-called stator iron back. Therefore, stator teeth and coil ends are excluded from the model. Furthermore, for further calculation, the density of the common-mode current as it enters the stator lamination stack from the stator winding is assumed to be homogeneous along the length of the stack length l_{Fe}. In fact, dv/dt decreases along the phase winding. Therefore, the flow of common-mode current across the stator winding insulation onto the lamination is not constant along the winding. However, averaging over one phase at a given distance from the end of the lamination stack into axial (z-) direction results in an approximately constant distribution of the common-mode current along the stack length (Fig. 4).

For frequencies of several 100 kHz, the skin depth δ_s is less than 50 μm and is much smaller than the thickness of a lamination sheet b_{Fe} of typically 0.5 mm. In this case, the lamination can be described by an analytical model for 1) one conducting half-plane, if the current enters from the stator slot
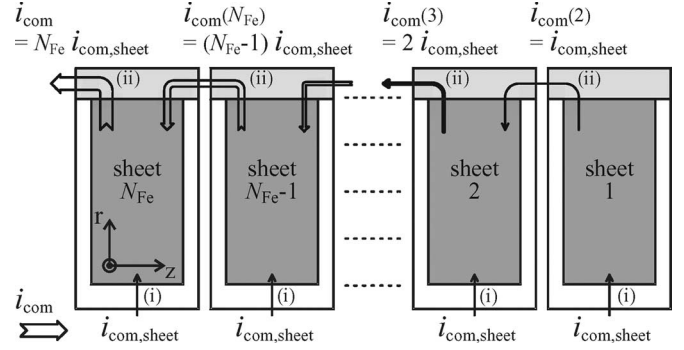

Fig. 5. Common-mode currents of individual sheets flowing from the stator winding [case (i)] and from the neighboring sheet [case (ii)].

and leaves through the stator housing, and 2) two conducting half-planes, if the current enters the sheet on one side of the stator housing and leaves at the other side through the stator housing. The field solution in one sheet with current flowing both from the winding and the neighboring sheet is given by superposition of the two models [11], [12] (Fig. 5).

With these assumptions, given the number of sheets of the stator core stack N_{Fe}, the inner and outer diameters of the stator lamination d_{si} and d_{se}, and the height of the stator slot h_s, the analytical solution of the common-mode flux is

$$\Phi_0 = \mu \frac{N_{\text{Fe}} i_{\text{com}}}{2\pi} \ln\left(\frac{d_{\text{se}}/2}{d_{\text{si}}/2 + h_s}\right) \frac{\delta_s}{\sqrt{2}}. \tag{1}$$

As the common-mode flux varies with time, it induces a voltage in the loop "stator frame–nondrive end–shaft–drive end" (Fig. 2), as expressed by

$$\begin{aligned} v_{\text{max}} &= 2\pi f \Phi_0 \\ &= \mu_0 \mu_r N_{\text{Fe}} \hat{i}_{\text{com}} f \ln\left(\frac{d_{\text{se}}/2}{d_{\text{si}}/2 + h_s}\right) \frac{\delta_s}{\sqrt{2}}. \end{aligned} \tag{2}$$

The number of sheets of the stator core stack N_{Fe} is proportional to the length of the stator core l_{Fe}, which is proportional to the frame size of a machine h. Furthermore, the stator winding-to-frame capacitance C_{wf} is proportional to h^2, i.e., the square of h, and the common-mode current i_{com} is approximately proportional to C_{wf} [13]. As the skin depths $\delta_s \propto 1/\sqrt{f \mu_r}$, the common-mode flux decreases with $1/\sqrt{f \mu_r}$, resulting in the following equations:

$$\Phi_0 \propto i_{\text{com}} l_{\text{Fe}} \propto h^3 \tag{3}$$

$$\Phi_0 \propto 1/\sqrt{f} \tag{4}$$

$$\Phi_0 \propto \sqrt{\mu_r} \tag{5}$$

$$v_{\text{max}} \propto i_{\text{com}} l_{\text{Fe}} \propto h^3 \tag{6}$$

$$v_{\text{max}} \propto \sqrt{f} \tag{7}$$

$$v_{\text{max}} \propto \sqrt{\mu_r}. \tag{8}$$

Both common-mode flux Φ_0 and induced voltage v increase with the cube of the frame size h. The frequency f has an

TABLE I
INVESTIGATED SQUIRREL-CAGE INDUCTION MOTORS (400 V, 50 Hz)

Power / kW	Poles	Frame Size / mm	Motors
11	4	160	M11a, M11b
110	4	280	M110a, M110b
500	6	400	M500a
	2	400	M500b

TABLE II
CALCULATED VALUES OF $\Phi_0/\hat{\imath}_{\mathrm{com}}$, $v_{\max}/\hat{\imath}_{\mathrm{com}}$, AND
$v_{\max}(1/\kappa_{\mathrm{Fe}} = 25 \cdot 10^{-8}\ \Omega \cdot \mathrm{m})$

Motor	M11a	M11b	M110a	M110b	M500a	M500b
$\Phi_0/\hat{\imath}_{\mathrm{com}}$/nWb/A ($f=100$ kHz, $\mu_{\mathrm{r}}=100$) and ($f=1$ MHz, $\mu_{\mathrm{r}}=1000$)	60.68	59.54	156.46	162.96	172.18	326.52
$\Phi_0/\hat{\imath}_{\mathrm{com}}$/nWb/A ($f=100$ kHz, $\mu_{\mathrm{r}}=1000$)	194.46	190.53	500.68	521.47	550.99	1044.86
$v_{\max}/\hat{\imath}_{\mathrm{com}}$/V/A ($f=100$ kHz, $\mu_{\mathrm{r}}=100$)	0.0381	0.0374	0.0983	0.1024	0.1082	0.2052
$v_{\max}/\hat{\imath}_{\mathrm{com}}$/V/A ($f=100$ kHz, $\mu_{\mathrm{r}}=1000$)	0.1220	0.1197	0.3146	0.3277	0.3462	0.6565
$v_{\max}/\hat{\imath}_{\mathrm{com}}$/V/A ($f=1$ MHz, $\mu_{\mathrm{r}}=1000$)	0.3812	0.3741	0.9831	1.0239	1.0819	2.0516
$\hat{\imath}_{\mathrm{com}}$/ A	3	4	19	24	60	40
$v_{\max}$/ V ($f=100$ kHz, $\mu_{\mathrm{r}}=100$)	0.11	0.15	1.87	2.46	6.49	8.21
$v_{\max}$/ V ($f=100$ kHz, $\mu_{\mathrm{r}}=1000$)	0.37	0.48	5.98	7.87	20.77	26.26
$v_{\max}$/ V ($f=1$ MHz, $\mu_{\mathrm{r}}=1000$)	1.14	1.5	18.68	24.57	64.91	82.06

inverse effect on the two parameters: The common-mode flux decreases, and the induced voltage increases with the root of f. Both parameters increase with the root of the relative permeability μ_{r}. It should be noted again that these statements refer to "conventional" machines where the understanding of the generation of the common-mode flux as described in [11] and [12] can be applied, as the common-mode current passes the stator stack lamination when leaving the machine.

Calculations were performed for six selected test motors from 11- to 500-kW rated power (Table I). Table II shows the calculated values of:

1) the ratio of common-mode flux Φ_0 versus amplitude of common-mode current $\hat{\imath}_{\mathrm{com}}$ ($\Phi_0/\hat{\imath}_{\mathrm{com}}$);
2) the ratio of induced voltage $v_{\max}$ versus amplitude of common-mode current $\hat{\imath}_{\mathrm{com}}$ ($v_{\max}/\hat{\imath}_{\mathrm{com}}$);
3) the amplitude of the induced voltage $v_{\max}$ for a typical measured amplitude of the common-mode current $\hat{\imath}_{\mathrm{com}}$.

Three pairs of frequency f and relative permeability μ_{r} were chosen:

(a) $f = 100$ kHz, $\mu_{\mathrm{r}} = 100$;
(b) $f = 100$ kHz, $\mu_{\mathrm{r}} = 1000$;
(c) $f = 1$ MHz, $\mu_{\mathrm{r}} = 1000$.

The results are shown in Table II.

1) $\Phi_0/\hat{\imath}_{\mathrm{com}}$: The value of $\Phi_0/\hat{\imath}_{\mathrm{com}}$ increases by a factor of $\sqrt{10} \approx 3.2$ from case (a) to case (b), according to (5), and decreases by the same factor from case (b) to case (c). Furthermore, the increase with motor size is noticeable. The two motors of the 11- and 110-kW power levels have the same number of poles; therefore, they have similar geometrical dimensions and approximately the same value of $\Phi_0/\hat{\imath}_{\mathrm{com}}$. This is not the case for the two motors of the 500-kW power level: motor M500a has six poles, and motor M500b has two poles. Thus, the ratio of stator lamination outer and inner diameters d_{se} and d_{si} is larger for motor M500b than for motor M500a, resulting in a larger value of $\Phi_0/\hat{\imath}_{\mathrm{com}}$.
2) $v_{\max}/\hat{\imath}_{\mathrm{com}}$: The ratio $v_{\max}/\hat{\imath}_{\mathrm{com}}$ increases by a factor of $\sqrt{10} \approx 3.2$ from case (a) to case (b), and case (b) to case (c), respectively, according to (7). The influence of motor size and number of poles of the motors is the same as for the value $\Phi_0/\hat{\imath}_{\mathrm{com}}$, as discussed previously in the text.
3) $v_{\max}$: As larger machines have larger common-mode currents [13], the induced voltage increases with about the cube of the motor size. It has to be noticed that the induced voltages $v_{\max}$ of the two motors of the 500-kW power level are in the *same range*, even if the values of $\Phi_0/\hat{\imath}_{\mathrm{com}}$ and $v_{\max}/\hat{\imath}_{\mathrm{com}}$ differ. As the ground current of M500a with the lower value of $v_{\max}/\hat{\imath}_{\mathrm{com}}$ is larger, the induced voltage is about the same as at motor M500b. Therefore, the significant influence of the number of poles on the magnitude of the induced voltage is found.

The model explains the occurrence of circulating bearing currents at larger motors [13]–[15]: At smaller motors, the calculated values of the induced voltage are only in the order of the threshold voltage of the bearing's lubrication film, where the bearings loose their insulating property. This value is exceeded at larger motors, and the circulating bearing currents can flow in the described loop.

III. CALCULATION OF CIRCULATING BEARING CURRENTS

A. Mutual Inductance of Ground and Bearing Current Path

With the high-frequency common-mode current i_{com} causing the common-mode flux Φ_0 that varies with time, thereby inducing a voltage v as described in Section II, and with the circulating bearing current flowing as a result of this voltage, the machine can be considered as a current transformer. The ratio $\hat{\imath}_{\mathrm{b}}/\hat{\imath}_{\mathrm{com}}$ is given by the compensation of the magnetomotive force of the two circuits. Therefore, in a first step, the mutual inductance L_{g} of the two circuits is calculated.

The expression for L_{g} for a given frequency $f = \omega/(2\pi)$ is derived from (1), using (9). Therefore, L_{g} is given by

$$\underline{V}_{\max} = j\omega\Phi_0 = \{R_{\mathrm{g}} + j\omega L_{\mathrm{g}}\} \cdot \underline{\hat{I}}_{\mathrm{com}} \tag{9}$$

$$L_{\mathrm{g}} = \frac{N_{\mathrm{Fe}}}{2} \frac{\mu}{\pi} \ln\left(\frac{d_{\mathrm{se}}/2}{d_{\mathrm{si}}/2 + h_{\mathrm{s}}}\right) \frac{\delta_{\mathrm{s}}}{2}. \tag{10}$$
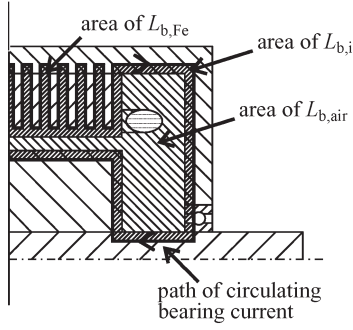
Fig. 6. Inductances of the path of the circulating bearing currents. For clarity, only half of the machine is shown.
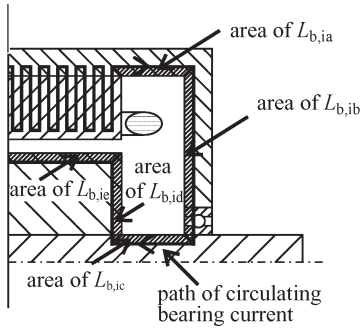

Fig. 7. Parts of the internal inductance $L_{b,i}$ of the path of the circulating bearing currents. For clarity, only half of the machine is shown.

B. Impedance of Bearing Current Path

First, the inductances along the bearing current paths are considered. Three different parts are distinguished (Fig. 6).

1) The first part is the internal inductance of the path through the stator lamination stack ($L_{b,Fe}$).
2) The second part is the self-inductance of the area enclosed by the circulating bearing current that is given by the air gap and the end-winding cavity ($L_{b,air}$).
3) The third part is the internal inductance of the bearing current path outside the stator lamination ($L_{b,i}$). Five parts contribute to the internal inductance of the path of the circulating bearing current outside the stator lamination stack (Fig. 7): a) frame outside stack ($L_{b,ia}$), b) end shield on drive end and nondrive end ($L_{b,ib}$), c) shaft outside the rotor lamination stack ($L_{b,ic}$), d) end sheet on drive end and nondrive end of the rotor lamination stack ($L_{b,id}$), and e) resurfaced rotor lamination stack ($L_{b,ie}$).

The three inductances $L_{b,Fe}$, $L_{b,air}$, and $L_{b,i}$ are given by (11)–(13), where d_{re} and d_{ri} are the outer and inner diameters of the rotor core, l_b is the distance between the two bearing seats, and δ_s^* is the skin depth of the materials of frame, end shields, and rotor shaft that are assumed to have the same permeability and electric conductivity. Hence, the inductance of the bearing current paths L_b is given by (14). The aforementioned equations are as follows:

$$L_{b,Fe} = \mu \frac{N_{Fe}}{\pi} \ln\left(\frac{d_{se}/2}{d_{si}/2 + h_s}\right)\frac{\delta_s}{2} = 2L_g \qquad (11)$$

$$L_{b,air} = \frac{\mu_0}{2\pi}\left\{\ln\left(\frac{d_{si}}{d_{re}}\right)l_{Fe} + \left(\frac{d_{se}}{d_{ri}}\right)(l_b - l_{Fe})\right\} \qquad (12)$$

TABLE III
CALCULATED INDUCTANCES L_g, $L_{b,Fe}$, $L_{b,air}$, $L_{b,i}$, AND L_b IN MICROHENRYS ($1/\kappa_{Fe} = 25 \cdot 10^{-8}\ \Omega \cdot m$)

Motor	M11a	M11b	M110a	M110b	M500a	M500b
L_g (f = 100 kHz, μ_r = 100) and (f = 1 MHz, μ_r = 1000)	0.043	0.042	0.111	0.116	0.122	0.231
L_g (f = 100 kHz, μ_r = 1000)	0.141	0.133	0.350	0.365	0.685	0.730
$L_{b,Fe}$ (f = 100 kHz, μ_r = 100) and (f = 1 MHz, μ_r = 1000)	0.086	0.084	0.221	0.231	0.244	0.462
$L_{b,Fe}$ (f = 100 kHz, μ_r = 1000)	0.281	0.266	0.399	0.729	0.770	1.460
$L_{b,air}$	0.073	0.048	0.065	0.097	0.191	0.277
$L_{b,i}$ (f = 100 kHz, μ_r = 100) and (f = 1 MHz, μ_r = 1000)	0.012	0.011	00.12	0.011	0.014	0.016
$L_{b,i}$ (f = 100 kHz, μ_r = 1000)	0.039	0.034	0.038	0.033	0.044	0.048
L_b (f = 100 kHz, μ_r = 100) and (f = 1 MHz, μ_r = 1000)	0.171	0.143	0.298	0.339	0.449	0.755
L_b (f = 100 kHz, μ_r = 1000)	0.393	0.348	0.802	0.859	1.005	1.785

$$L_{b,i} = \frac{\mu\delta_s^*}{4\pi}\left\{\frac{l_b - l_{Fe}}{d_{se}/2} + 2\ln\left(\frac{d_{se}/2}{d_{ri}/2}\right) + \frac{l_b - l_{Fe}}{d_{ri}/2}\right.$$
$$\left. + 2\ln\left(\frac{d_{re}/2}{d_{ri}/2}\right)\right\} + \frac{\mu\delta_s}{4\pi}\frac{l_{Fe}}{d_{re}/2} \qquad (13)$$

$$L_b = L_{b,Fe} + L_{b,air} + L_{b,i}. \qquad (14)$$

Table III shows the calculated values of the five inductances L_g, $L_{b,Fe}$, $L_{b,air}$, $L_{b,i}$, and L_b of the circulating bearing path for the three pairs of frequency f and relative permeability μ_r already considered in Section II. For simplification, frame, end shields, and shaft are assumed to have the same relative permeability μ_r^*. The value of μ_r^* is about 100. It is an order of magnitude smaller than μ_r of the lamination, which reaches values up to several 1000. For simplification, the frame, end shields, and shaft are assumed to have the same relative permeability μ_r^*. Therefore, the internal inductance $L_{b,i}$ is calculated to be too large. However, the contribution of the inductance $L_{b,i}$ is negligible when compared with the other two inductances $L_{b,Fe}$ and $L_{b,air}$.

Next, the resistances along the path are considered. Three resistances are distinguished:

1) resistance of the path through the stator lamination $R_{b,Fe}$;
2) bearing resistance R_b;
3) resistance of the path outside the stator lamination except for the bearing resistance $R_{b,i}$.

The resistance along the path through the stator lamination $R_{b,Fe}$ is derived from (1) and (9) and is given by

$$R_{b,Fe} = N_{Fe}\frac{\omega\mu}{\pi}\ln\left(\frac{d_{se}/2}{d_{si}/2 + h_s}\right)\frac{\delta_s}{2} = \omega L_{b,Fe}. \qquad (15)$$

Table IV shows the calculated values of $R_{b,Fe}$ for the aforementioned three pairs of frequency f and relative permeability μ_r.

TABLE IV
CALCULATED RESISTANCES $R_{\mathrm{b,Fe}}$ IN MILLIOHMS
$(1/\kappa_{\mathrm{Fe}} = 25 \cdot 10^{-8}\ \Omega \cdot \mathrm{m})$

Motor	M11a	M11b	M110a	M110b	M500a	M500b
$R_{\mathrm{b,Fe}}$ ($f=100$ kHz, $\mu_{\mathrm{r}}=100$)	53.9	52.9	139.0	144.8	154.0	290.1
$R_{\mathrm{b,Fe}}$ ($f=100$ kHz, $\mu_{\mathrm{r}}=1000$)	170.5	167.3	439.7	457.9	483.8	917.5
$R_{\mathrm{b,Fe}}$ ($f=1$ MHz, $\mu_{\mathrm{r}}=1000$)	539.2	529.1	1390.3	1448.0	1540.0	2901.4

TABLE V
CALCULATED RATIOS $|\hat{I}_{\mathrm{b}}/\hat{I}_{\mathrm{com}}|$ (WITHOUT COPPER LOOP)
AND $|\hat{I}_{\mathrm{bL}}/\hat{I}_{\mathrm{com}}|$ (WITH COPPER LOOP)

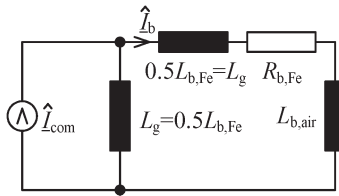| Motor	M11a	M11b	M110a	M110b	M500a	M500b
$|\hat{I}_{\mathrm{b}}/\hat{I}_{\mathrm{com}}|$ ($f=100$ kHz, $\mu_{\mathrm{r}}=100$) and ($f=1$ MHz, $\mu_{\mathrm{r}}=1000$)	0.24	0.27	0.29	0.29	0.24	0.27
$|\hat{I}_{\mathrm{b}}/\hat{I}_{\mathrm{com}}|$ ($f=100$ kHz, $\mu_{\mathrm{r}}=1000$)	0.31	0.32	0.33	0.33	0.31	0.32
$|\hat{I}_{\mathrm{bL}}/\hat{I}_{\mathrm{com}}|$ ($f=100$ kHz, $\mu_{\mathrm{r}}=100$) and ($f=1$ MHz, $\mu_{\mathrm{r}}=1000$)	0.11	0.12	0.19	0.20	0.18	0.22
$|\hat{I}_{\mathrm{bL}}/\hat{I}_{\mathrm{com}}|$ ($f=100$ kHz, $\mu_{\mathrm{r}}=1000$)	0.22	0.23	0.29	0.29	0.28	0.30
$|(\hat{I}_{\mathrm{bL}}\text{-}\hat{I}_{\mathrm{b}})/\hat{I}_{\mathrm{com}}|$ ($f=100$ kHz, $\mu_{\mathrm{r}}=100$) and ($f=1$ MHz, $\mu_{\mathrm{r}}=1000$)	-51 %	-54 %	-38 %	-30 %	-27 %	-17 %
$|(\hat{I}_{\mathrm{bL}}\text{-}\hat{I}_{\mathrm{b}})/\hat{I}_{\mathrm{com}}|$ ($f=100$ kHz, $\mu_{\mathrm{r}}=1000$)	-28 %	-29 %	-13 %	-13 %	-12 %	-7 %

Fig. 8. Equivalent circuit for calculation of circulating bearing currents.

The bearing resistance R_{b} is estimated according to [16]. As the circulating bearing currents have peak amplitudes of several amperes, numerous conduction bridges are built up, and the bearing resistance is assumed to value less than 10 mΩ. Therefore, it is negligible when compared with the resistance $R_{\mathrm{b,Fe}}$.

In the same way as the inductance $L_{\mathrm{b,i}}$, the resistance $R_{\mathrm{b,i}}$ of the path through the stator lamination comprises five parts, i.e., $R_{\mathrm{b,ia}}$ to $R_{\mathrm{b,ie}}$, corresponding to the parts that give the internal inductances $L_{\mathrm{b,ia}}$ to $L_{\mathrm{b,ie}}$. In a similar way as $L_{\mathrm{b,i}}$, $R_{\mathrm{b,i}}$ is also negligible when compared with $R_{\mathrm{b,Fe}}$. Therefore, $R_{\mathrm{b}} \cong R_{\mathrm{b,Fe}}$.

C. Ratio of Circulating Bearing Current and Common-Mode Current

The circulating bearing current and the common-mode current path are coupled via the common-mode flux. The transformation ratio is given by the ratio of the respective impedances (Fig. 8), i.e.,

$$\left|\frac{\hat{\underline{I}}_{\mathrm{b}}}{\hat{\underline{I}}_{\mathrm{com}}}\right| = \left|\frac{j\omega L_{\mathrm{g}}}{R_{\mathrm{g,Fe}} + j\omega L_{\mathrm{b,Fe}} + j\omega L_{\mathrm{b,air}}}\right|$$
$$= 0.5\sqrt{\frac{1}{(1 + X_{\mathrm{b,air}}/X_{\mathrm{b,Fe}})^2 + 1}}. \quad (16)$$

IV. RESULTS

A. Ratio $|\hat{\underline{I}}_{\mathrm{b}}/\hat{\underline{I}}_{\mathrm{com}}|$ Without Measurement of Bearing Currents

The ratio $|\hat{\underline{I}}_{\mathrm{b}}/\hat{\underline{I}}_{\mathrm{com}}|$ is calculated for three pairs of frequency f and relative permeability μ_{r} and the six test motors described in Section II. The results are shown in Table V.

As L_{g} and $L_{\mathrm{b,Fe}}$ depend on f and μ_{r}, whereas $L_{\mathrm{b,air}}$ is independent of these parameters, the ratio $|\hat{I}_{\mathrm{b}}/\hat{I}_{\mathrm{com}}|$ increases with increasing relative permeability μ_{r} and decreases with increasing frequency f.

B. Ratio $|\hat{\underline{I}}_{\mathrm{bL}}/\hat{\underline{I}}_{\mathrm{com}}|$ With Measurement of Bearing Currents

For measurement purposes, an insulating layer is inserted into the end shields of the test motors close to the bearing seat. This insulating layer is bridged by a small copper loop for measurement of the bearing currents with high-frequency current probes. The measured value of the inductance of the copper loop is $L_{\mathrm{cu}} = 0.1\ \mu$H. The capacitance of the insulating layer is in the order of 1–5 nF. For frequencies of several 100 kHz, the parallel capacitive impedance given by the insulating layer is much larger than the inductive impedance of the copper loop. Therefore, it is neglected, and the ratio $|\hat{\underline{I}}_{\mathrm{bL}}/\hat{\underline{I}}_{\mathrm{com}}|$, where $\hat{I}_{\mathrm{bL}}$ is the bearing current amplitude with consideration of the copper loop for measurement of bearing currents, is given by

$$\left|\frac{\hat{\underline{I}}_{\mathrm{bL}}}{\hat{\underline{I}}_{\mathrm{com}}}\right| = 0.5\sqrt{\frac{1}{(1 + X_{\mathrm{b,air}}/X_{\mathrm{b,Fe}} + 2X_{\mathrm{cu}}/X_{\mathrm{b,Fe}})^2 + 1}}. \quad (17)$$

The ratio $|\hat{I}_{\mathrm{bL}}/\hat{I}_{\mathrm{com}}|$ is calculated for three pairs of frequency f and relative permeability μ_{r} described in Section II. The results are also given in Table V. Depending on the values of f and μ_{r}, the copper loop for measurement of the bearing currents reduces the circulating bearing currents at the 110-kW power level by 13% to 38% and at the 500-kW power level by 7% to 27%. For the motors of the 11-kW power level, these calculations are not of importance, as no circulating bearing current flow occurs.

The theoretical results are compared with measurement results that have been obtained in the frame of a research program for systematic investigation of the influence of system parameters on parasitic bearing currents during inverter operation [13], [14]. The experimental results for inverter-fed squirrel-cage motors with 110- and 500-kW rated powers are shown in Figs. 9 and 10, respectively. These measurements were performed during no-load operation. The shaft-mounted fans were removed to achieve bearing temperatures that are typical for
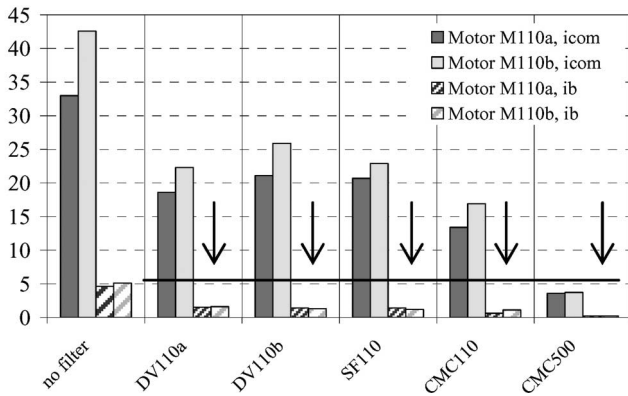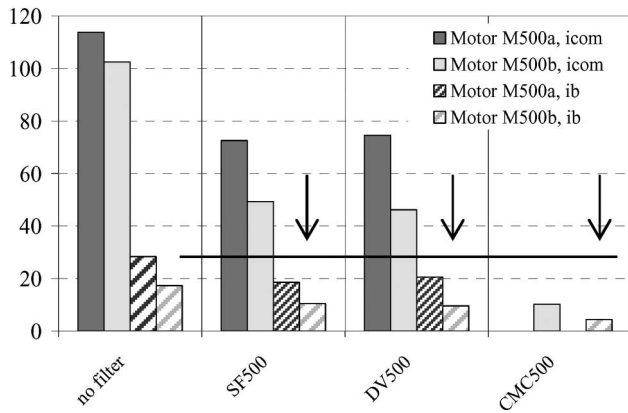
Current / A peak-to-peak

Fig. 9. Power level of 110 kW. Measured common-mode currents and bearing currents with filters, motor speed $n = 15/\text{min}$, bearing temperature $\vartheta_\text{b} \approx 70$ °C, 10-m shielded motor cable, DV = dv/dt-reactor, SF = sinusoidal filter, and CMC = common-mode choke [14].

Current / A peak-to-peak

Fig. 10. Power level of 500 kW. Measured common-mode currents and bearing currents with filters, motor speed $n = 15/\text{min}$, bearing temperature $\vartheta_\text{b} \approx 70$ °C, 10-m motor shielded cable, DV = dv/dt-reactor, SF = sinusoidal filter, and CMC = common-mode choke [14].

loaded operation ($\vartheta_\text{b} = 70{-}80$ °C). For each operating point, large numbers of measurement samples (> 30) were recorded with a time window of 8 ms per sample. Average peak-to-peak values were calculated using the maximum values in each stored waveform in order to get statistically reliable results. The low motor speed of $n = 15/\text{min}$ in Figs. 9 and 10 has been selected because the bearing has minimum resistance in the low-speed region. Thus, the largest values of the circulating bearing currents occur in the low-speed region. It should be noted that this is considered by the model via the very small value of R_b, as discussed in Section IV-B. In Figs. 9 and 10, the ratio of common-mode current and bearing current can be derived from the measurement results. Both the results for drive operation with and without the use of different inverter output filters are shown. With the use of filters, the common-mode current is reduced (e.g., [14] and [17]). This translates into a reduction of the circulating bearing currents to a similar degree, as the ratio between common-mode current and circulating bearing current is the same for both types of drive operation.

The ratios of common-mode current versus circulating bearing current obtained from the measurements are summarized as follows:

$$|\hat{\underline{I}}_\text{bL}/\hat{\underline{I}}_\text{com}|_\text{measured} = 0.2 - 0.3. \qquad (18)$$

The theoretical and measurement results are well in line.

C. Maximum Ratio $|\hat{\underline{I}}_\text{b}/\hat{\underline{I}}_\text{com}|$

As a result of the presented approach, the theoretical maximum ratio of circulating bearing current and common-mode current is 0.354, as shown in the following:

$$\max\left\{\left|\frac{\hat{\underline{I}}_\text{b}}{\hat{\underline{I}}_\text{com}}\right|\right\} = \lim_{X_\text{b,air} \to 0}\left\{0.5\sqrt{\frac{1}{(1 + X_\text{b,air}/X_\text{b,Fe})^2 + 1}}\right\}$$
$$= 0.5\sqrt{\frac{1}{2}} = 0.354. \qquad (19)$$

V. SUMMARY

The induction of high-frequency circulating bearing currents in inverter-based machines can be described by an eddy-current model and by parameters of an equivalent circuit derived from the model. The model explains the occurrence of circulating bearing currents at larger motors. The theoretical maximum ratio of circulating bearing current and common-mode current is about 0.35. Copper loops, which can be used for measurement of the bearing currents, decrease the circulating bearing currents at motors of 110- and 500-kW rated powers by about 10% to 40%, depending on the frequency of the current and the relative permeability of the stator lamination stack.

REFERENCES

[1] S. Chen, T. A. Lipo, and D. Novotny, "Circulating type motor bearing current in inverter drives," in *Proc. 32nd IEEE Ind. Appl. Soc. Annu. Meeting*, 1996, vol. 1, pp. 162–166.
[2] J. Ollila, T. Hammar, J. Lisakkala, and H. Tuusa, "A new reason for bearing current damages in variable speed drives," in *Proc. 7th EPE*, Trondheim, Norway, 1997, pp. 2539–2542.
[3] A. Binder, R. Aust, and A. Schrepfer, "Bearing currents—A danger to inverter-fed AC-motors?" *Iron Steel Eng.*, vol. 76, no. 7, pp. 47–52, Jul. 1999.
[4] P. J. Link, "Minimizing electric bearing currents in ASD systems," *IEEE Ind. Appl. Mag.*, vol. 5, no. 4, pp. 55–66, Jul./Aug. 1999.
[5] H.-J. Conraths, F. Gießler, and H.-D. Heining, "Shaft-voltages and bearing currents—New phenomena in inverter driven induction machines," in *Proc. 8th Eur. Conf. Power Electron. Appl. (EPE)*, Lausanne, Switzerland, 1999, CD-ROM, Paper 165.
[6] V. Hausberg and H.-O. Seinsch, "Wellenspannungen und zirkulierende Lagerstroeme bei umrichtergespeisten Induktionsmaschinen," *Elect. Eng.*, vol. 82, pp. 313–326, 2000.
[7] H. E. Boyanton and G. Hodges, "Bearing fluting," *IEEE Ind. Appl. Mag.*, vol. 8, no. 5, pp. 53–57, Sep./Oct. 2002.
[8] R. F. Schiferl and M. J. Melfi, "Bearing current remediation options," *IEEE Ind. Appl. Mag.*, vol. 10, no. 4, pp. 40–50, Jul./Aug. 2004.
[9] S. Ogasawara and H. Akagi, "Modeling and damping of high-frequency leakage currents in PWM inverter-fed AC motor drive systems," *IEEE Trans. Ind. Appl.*, vol. 32, no. 5, pp. 1105–1114, Sep./Oct. 1996.
[10] P. Maeki-Ontto and J. Luomi, "Bearing current prevention of converter-fed AC machines with a conductive shielding in stator slots," in *Proc. 4th IEMDC*, Madison, WI, 2003, vol. 1, pp. 247–278.

[11] ——, "Common mode flux calculation of AC machines," in *Proc. 15th Int. Conf. Electr. Mach. Drives (ICEM)*, Bruges, Belgium, 2002, CD-ROM, Paper 549.

[12] ——, "Circumferential flux as a source of bearing current of converter-fed AC machines," in *Proc. NORPIE*, Stockholm, Sweden, 2002, CD-ROM.

[13] A. Muetze, "Bearing currents in inverter-fed AC motors," Ph.D. dissertation, Darmstadt Univ. Technol., Aachen, Germany, 2004.

[14] A. Muetze and A. Binder, "Don't lose your bearings—Mitigation techniques for bearing currents in inverter-supplied drive systems," *IEEE Ind. Appl. Mag.*, vol. 12, no. 4, pp. 22–31, Jul./Aug. 2006.

[15] ——, "Practical rules for assessment of inverter-in-duced bearing currents in inverter-fed AC-motors up to 500 kW," in *Proc. 16th Int. Conf. Electr. Mach. Drives (ICEM)*, Krakow, Poland, 2004, CD-ROM, Paper 281.

[16] H. Prashad, "Effect of operating parameters on the threshold voltages and impedances response of non-insulated rolling element bearings under the action of electrical currents," *Wear*, vol. 117, pp. 223–239, 1987.

[17] H. Akagi and S. Tamura, "A passive EMI filter for elimination both bearing current and ground leakage current from an inverter-driven motor," *IEEE Trans. Power Electron.*, vol. 21, no. 5, pp. 1459–1469, Sep. 2006.

Annette Muetze (S'03–M'04) received the Dipl.-Ing. degree in electrical engineering from Darmstadt University of Technology, Darmstadt, Germany, in 1999, the degree in General Engineering from the Ecole Centrale de Lyon, Ecully, France, in 1999, and the Dr. Tech. degree in electrical engineering from Darmstadt University of Technology in 2004, under the supervision of Prof. A. Binder.

In May 2004, she joined the Department of Electrical and Computer Engineering, University of Wisconsin, Madison, as an Assistant Professor. Since January 2007, she has been a Lecturer in the School of Engineering, University of Warwick, Coventry, U.K.

Dr. Muetze received a National Science Foundation CAREER Award in 2005. Her work on inverter-induced bearing currents has been awarded with the FAG Innovation Award 2004.

Andreas Binder (M'97–SM'04) received the Dipl.-Ing. and Dr. Tech. degrees in electrical engineering from the University of Technology, Vienna, Austria, in 1981 and 1988, respectively.

From 1981 to 1983 he was with ELIN-Union AG, Vienna, where he worked on synchronous generators design. From 1983 to 1989, he was a Researcher in the Department of Electrical Machines and Drives, University of Technology, Vienna. From 1989 to 1997, he led a group in developing dc and inverter-fed ac motors and drives at Siemens AG, Bad Neustadt and Erlangen, Germany. Since 1994, he has been a Lecturer at the University of Technology, Vienna (*venia docendi*). Since October 1997, he has been the Head of the Institute of Electrical Energy Conversion, Darmstadt University of Technology, Darmstadt, Germany, as a Full Professor, where he is responsible for teaching and conducting research on electrical machines, drives, and railway systems. He is the author or coauthor of 120 scientific publications and is the holder of several patents.

Prof. Binder has been the Head of the Electrical Machines, Drives, and Mechatronics Section, German Association of Electrical Engineers (VDE), since 1999. He is a recipient of the ETG-Literature Award from the VDE in 1997.